INTERNATIONAL JOURNAL FOR NUMERICAL AND ANALYTICAL METHODS IN GEOMECHANICS
Int. J. Numer. Anal. Meth. Geomech. 2010; **34**:533–549
Published online 1 September 2009 in Wiley InterScience (www.interscience.wiley.com). DOI: 10.1002/nag.831

Mechanical and transport constitutive models for fractures subject to dissolution and precipitation

Derek Elsworth[1,*,†] and Hideaki Yasuhara[2]

[1]*Department of Energy and Mineral Engineering, Penn State University, University Park, PA 16802, U.S.A.*
[2]*Department of Civil and Environmental Engineering, Ehime University, 3, Bunkyo-cho, Matsuyama 790-8577, Japan*

SUMMARY

Transient changes in the permeability of fractures in systems driven far-from-equilibrium are described in terms of proxy roles of stress, temperature and chemistry. The combined effects of stress and temperature are accommodated in the response of asperity bridges where mineral mass is mobilized from the bridge to the surrounding fluid. Mass balance within the fluid accommodates mineral mass either removed from the flow system by precipitation or advection, or augmented by either dissolution or advection. Where the system is hydraulically closed and initially at equilibrium, reduction in aperture driven by the effects of applied stresses and temperatures will be augmented by precipitation on the fracture walls. Where the system is open, the initial drop in aperture may continue, and accelerate, where the influent fluid is oversaturated with respect to the equilibrium mineral concentration within the fluid, or may reverse, if undersaturated. This simple zero-dimensional model is capable of representing the intricate behavior observed in experiments where the feasibility of fracture sealing concurrent with net dissolution is observed. This zero-order model is developed as a constitutive model capable of representing key aspects of changes in the transport parameters of the continuum response of fractured media to changes in stress, temperature and chemistry. Copyright © 2009 John Wiley & Sons, Ltd.

Received 11 January 2008; Revised 24 November 2008; Accepted 20 July 2009

KEY WORDS: permeability; precipitation and dissolution; fractures; pressure solution

1. INTRODUCTION

The evolution of transport characteristics in fractured rocks is controlled by competition between the chemical and mechanical effects that either generate (including dilatant shear, microcracking,

*Correspondence to: Derek Elsworth, Department of Energy and Mineral Engineering, Penn State University, University Park, PA 16802, U.S.A.
†E-mail: elsworth@psu.edu

Contract/grant sponsor: US Department of Energy; contract/grant number: DE-AC02-05CH11231
Contract/grant sponsor: National Science Foundation; contract/grant number: EAR-0510182

thermal cracking and focused dissolution) or destroy (including shear and hydrostatic compaction, fracture healing, dislocation creep and pressure solution prompted by water-film and free-face diffusion) porosity. Crucial in this understanding of chemical effects are the mechanisms through which mechanical deformation contributes to changes in permeability, and by which the mechanical response in turn is modified. These effects are especially important in fractured rocks, where both permeability and stiffness are intrinsically controlled by the most hydraulically conductive, and most mechanically soft, elements, viz. the fractures.

These effects are known to be important at relatively modest stresses, temperatures, and typically for systems pushed far from chemical equilibrium, such as in geothermal or hydrocarbon reservoirs or around waste repositories. Sealing is suggested in some instances of vapor and fluid transport under low [1–3] and moderate stresses [4] and gaping is suggested in the acidizing literature of the petroleum field [5–7] and in the development of karst [8–11]. The controlling processes and feedbacks apply in varying degree at a variety of spatial and temporal scales. These include our understanding of diagenetic processes at basin scale [12–15], where the implicated minerals comprising the aggregate may be quartz [16–18], halite [19], feldspars [20], calcite [9, 21] or clays [22, 23], and where veining [24] or crack sealing [22, 25–27], or the timing of the earthquake cycle [28–36] is affected by the evolution of mechanical and transport properties. These properties may relate to granular [37–39] or fractured media [40–42], and may be moderated by the effects of chemical response [41, 43] or of brittle deformation [37, 44]. In all cases, the processes and feedbacks apparent in these complex systems are wide ranging and have broad significance.

Key issues in this understanding relate to the strength and sense of various feedbacks, and their influence in defining the effect of reactive mass transport on permeability change. Important questions remain regarding the magnitude of anticipated changes in permeability or stiffnesses in response to these coupled chemical and mechanical effects, and indeed their sense. Enigmatically, systems subject to compressive loads and net chemical dissolution have been observed to gape, rather than to seal [8, 10, 11] and others to seal rather than to gape [2, 41, 42]. These systems are under nominally similar stresses, but differ principally in paths of temperature or evolving chemical potential. The key issue relates to mobility of solid mineral matter comprising the fracture surfaces and in the source and destination for the redistribution of mineral mass that contributes to these changes.

This work presents relationships describing the evolution of permeability based on mechanistically consistent but idealized models of contacting fractures to define the evolution of transport and mechanical properties with paths of chemical potential.

2. MECHANISTIC MODEL

This model describes the behavior of a system subject to the serial effects of pressure solution, free-face dissolution and precipitation and dissolution, including advection from the control volume. To describe behavior, we evaluate closure of the fracture driven by pressure solution, to a new equilibrium configuration as controlled by a specific contact model. This closure of the fracture is a function of pressure solution only, and is not influenced by an undercutting mechanism of free-face dissolution. As the system approaches this equilibrium configuration, it may be acted upon by free-face dissolution, with material advected from the system.

DOI: 10.1002/nag

2.1. Contact model

Closure between two contacting rough fracture surfaces, as illustrated in Figure 1, is driven by a change in the applied effective stress. The average normal stress, $\bar{\sigma}$, acting over a nominal area of the fracture, $\bar{R}$, results in a local asperity stress, σ_f, beneath the equilibrium contact area, R_f, as,

$$R_f = \bar{R}\frac{\bar{\sigma}}{\sigma_f} \tag{1}$$

The equilibrium contact area of the fracture is defined by the equilibrium stress, σ_f, as [39]

$$\sigma_f = \frac{E_m(1-T/T_m)}{4V_m} \tag{2}$$

where T is the ambient temperature, T_m the temperature of fusion, E_m the heat of fusion and V_m the molar volume of the mineral comprising the fracture asperity. The total volume removed as the fracture adjusts to a new equilibrium stress, σ_f, that is related to a new equilibrium contact area, R_f, must be determined from the architecture of the fracture porosity. The equivalent aperture, $\langle b\rangle$, may be defined in terms of residual aperture, b_r, and 'reference stress' aperture, b_0, in terms of [41, 43]

$$\langle b\rangle = b_\mathrm{r} + (b_0 - b_\mathrm{r})\mathrm{e}^{-(R_c - R_{c_0})a} \tag{3}$$

where R_{c_0} is the relative contact area at the reference stress (relative contact area is the ratio of fracture contact area to the total fracture area $\bar{R}$) and R_c is the relative equilibrium contact area, a defines the form of the contact-area-aperture relationship and $\langle b\rangle$ is the mean aperture. If the equilibrium stress is defined from Equation (2), and the equilibrium contact area from Equation (1), then the volume lost during fracture closure, V, may be determined as

$$\begin{aligned} V &= -A_f\int_{b_i}^{b_f}\frac{R_c}{1-R_c}\,\mathrm{d}\langle b\rangle = -A_f\int_{R_i}^{R_f}\frac{R_c}{1-R_c}\frac{\mathrm{d}\langle b\rangle}{\mathrm{d}R_c}\,\mathrm{d}R_c \\ &= A_f(b_0-b_\mathrm{r})\mathrm{e}^{-(1-R_{c_0})a}(\mathrm{e}^{-(1-R_f)a} - \mathrm{e}^{-(1-R_i)a} - a\mathrm{Ei}((1-R_f)a) + a\mathrm{Ei}((1-R_i)a)) \end{aligned} \tag{4}$$

where $\mathrm{Ei}(x)$ is the exponential integral function and A_f is the plan area of the fracture. Hence, the product of the 2-D total plan area of the fracture (A_f) and the proportion of this fracture, which contacts ($R_c/(1-R_c)$), defines the actual area of the asperities in contact. Multiplying this by the closure of the two fracture faces from an initial aperture, b_i, to a final aperture, b_f, defines the lost volume of fracture wall in the overlap. This evaluates the loss of material, which must occur as the opposing walls of the fracture interpenetrate, due to pressure-solution-like closure of the fracture, and enables the volume of mineral removed to be directly determined.

2.2. Pore-void continuity

The idealized geometry of the contacting fracture is shown in Figure 2. The mass of mineral removed from the asperity by stress-enhanced dissolution is ejected into the fluid within the pore volume, V_p. This mass is dissolved within the fluid, but is also available to be precipitated onto the pore (fracture) walls, or advected from the control volume. Assuming that the closure at the asperities is rate-controlled by dissolution beneath the contacting fracture asperity, then the rate of closure may be fitted to first order to an expression representing exponential decay. This is predicated on the exponentially diminishing rate of fracture closure observed in experiments with

DOI: 10.1002/nag

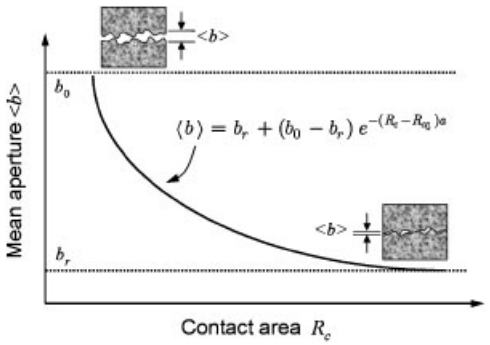

Figure 1. Contact model for two interpenetrating fracture surfaces. Model corresponds to Equation (3).

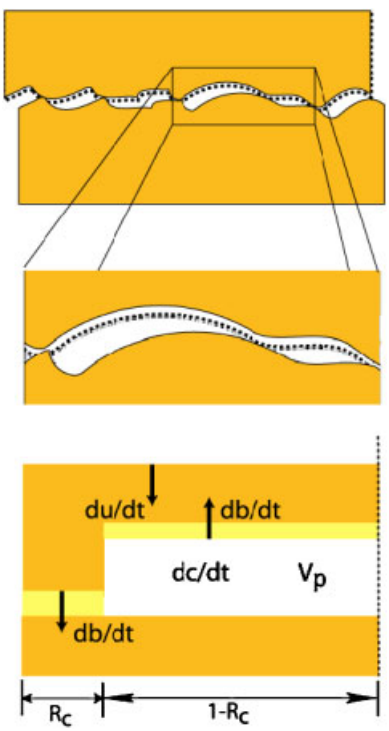

Figure 2. (Top) Geometry of contacting fracture walls. (Center) Fracture void is fluid filled. REV is defined within fracture geometry and closure occurs as facing fracture walls interpenetrate. (Bottom) Idealization of a fracture. Fracture void of volume V_p and proportional contact area R_c. Mass concentration changes within the void, $\mathrm{d}c/\mathrm{d}t$, and results in a change in the fracture aperture ($\mathrm{d}b/\mathrm{d}t$) due to dissolution under the anvil and on the free face, and closure of the system at rate $\mathrm{d}u/\mathrm{d}t$.

step-augmented temperatures (or stresses) with constant mass concentration held in the surrounding fluid (e.g. Figure 3). In a closed system with no free-face precipitation, the concentration within the stagnant fluid must build as $\mathrm{d}c/\mathrm{d}t = A\mathrm{e}^{-Ft}$, where the pre-exponential factor, A, and exponent

DOI: 10.1002/nag

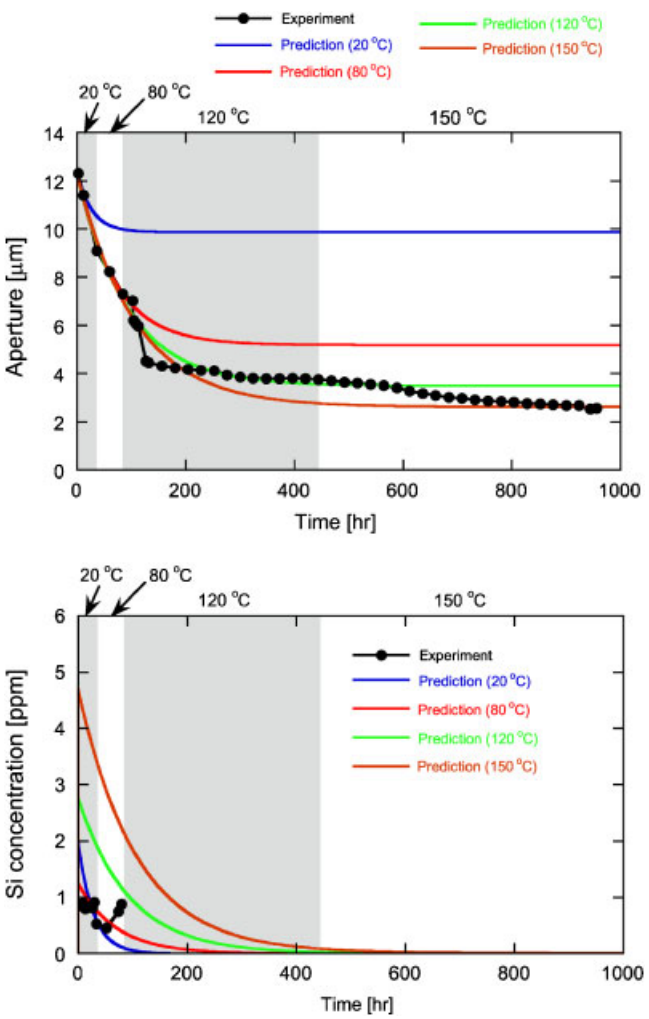

Figure 3. Data from a 1000 h flow-through test on a fracture in novaculite. Effective confining stress of ~2 MPa held constant and temperature incremented from 20°, from 80°, to 120°, to 150°C. Modeled results are for the parameters defined in Table I. (Top) Change in aperture with time. Sudden drop in aperture is due to excursion in pressure with pump failure. Closure history data with temperature are anchored to zero time, but may be translated in time to accommodate the resulting change in aperture. (Bottom) Change in Si concentration with time.

are fitting parameters. Note that this factor A must have units of mass-rate per unit volume, and is not the same as A_f. This first-order fitting of observed response is a key step in moving from the asperity scale to the continuum scale, and is followed here. From mass conservation, the change in concentration within the fluid may be defined as

$$\frac{\mathrm{d}c}{\mathrm{d}t} - A\mathrm{e}^{-Ft} + B(c - c_{\mathrm{eq}}) + Q(c - c_{\mathrm{in}}) = 0 \tag{5}$$

DOI: 10.1002/nag

where the evolving average fluid concentration within the REV, c, with time, t, is controlled relative to the equilibrium concentration of the fluid at a prescribed temperature and pressure, c_{eq}, and influent concentration, c_{in}, through constants representing the magnitude of pressure dissolution, A, the rate of pressure dissolution, F, the rates of free-face precipitation and dissolution, B and the mass flux, Q, defined in pore volumes per unit time.

This relationship assumes that: (1) pressure dissolution advances by dissolution at the contacts and is rate-controlled by dissolution, rather than by interface diffusion; (2) free-face dissolution or precipitation may be represented by the simple first-order rate law of $B(c-c_{\mathrm{eq}})$ with the term B incorporating constant (over an appropriate interval of stress and temperature) magnitudes of dissolution rate constants and reactive surface area; and (3) the fracture void REV is treated as a well-mixed reactor, with the constant fluid concentration defined throughout, and invaded by influent fluid at concentration c_{in}.

Although a simplified representation of average conditions in the fracture REV, Equation (5) nevertheless is able to capture the essential behaviors apparent in the pressure dissolution-driven response of fractures: that fractures may switch between closure and gaping as the stress or temperature boundary conditions are changed, and that typical features such that the long tailing in fracture closure may be followed even after aqueous concentrations have substantially reached equilibrium.

Where only the effects of pressure solution are considered, the volume removed by pressure solution may be defined as V_{ps}, by augmenting the concentration in the pore fluid by an amount, c_{ps}, and the rate of removal as

$$\frac{\mathrm{d}V_{\mathrm{ps}}}{\mathrm{d}t}=\frac{\mathrm{d}c_{\mathrm{ps}}}{\mathrm{d}t}\frac{V_p}{\rho} \tag{6}$$

and from Equation (5), $\mathrm{d}c_{\mathrm{ps}}/\mathrm{d}t=A\mathrm{e}^{-Ft}$. Substituting this into Equation (6) yields

$$V=\int_0^\infty \frac{\mathrm{d}V_{\mathrm{ps}}}{\mathrm{d}t}\,\mathrm{d}t=\frac{V_p}{\rho}\int_0^\infty A\mathrm{e}^{-Ft}\,\mathrm{d}t=\frac{V_p}{\rho}\frac{A}{F} \tag{7}$$

Equating this with the mass removed from the asperity (Equation (4)) enables the magnitude of A to be determined, and the rate of closure is conditioned by F. This ultimate volume removed into solution is equivalent to the product of equilibrium concentration, $c[t]=c[\infty]=A/F$, and V_p/ρ as identified in Equation (7).

2.3. System response

The response of the system to changes in pore fluid concentration may be determined from consideration of the combined effects of pressure dissolution, precipitation/dissolution and advection. For an REV, this is defined through the solution of

$$\frac{\mathrm{d}c}{\mathrm{d}t}\underbrace{-A\mathrm{e}^{-Ft}}_{-\mathrm{d}c_A/\mathrm{d}t}+\underbrace{B(c-c_{\mathrm{eq}})}_{-\mathrm{d}c_B/\mathrm{d}t}+\underbrace{Q(c-c_{\mathrm{in}})}_{-\mathrm{d}c_Q/\mathrm{d}t}=0 \tag{8}$$

where the components representing the processes of pressure solution ($\mathrm{d}c_A/\mathrm{d}t$), precipitation/dissolution ($\mathrm{d}c_B/\mathrm{d}t$) and advection ($\mathrm{d}c_Q/\mathrm{d}t$) are defined sequentially. Solving Equation (8) for

DOI: 10.1002/nag

the initial conditions of $c=c_0$ at $t=0^+$ yields

$$c[t]=\mathrm{e}^{-(B+Q)t}\left[\frac{A}{(B+Q-F)}(\mathrm{e}^{(B+Q-F)t}-1)+\frac{B}{(B+Q)}(c_0-c_{\mathrm{eq}}(1-\mathrm{e}^{(B+Q)t}))\right.$$
$$\left.+\frac{Q}{(B+Q)}(c_0-c_{\mathrm{in}}(1-\mathrm{e}^{(B+Q)t}))\right] \tag{9}$$

The change in displacement, u, driven by this process may be directly evaluated from the shortening of the supporting rock pedestal covering a proportion of the total area, R_c, as illustrated in Figure 2. The updated displacement is given as

$$u=u_i+\Delta u=u_i+\int_0^t\frac{\mathrm{d}u}{\mathrm{d}t}\mathrm{d}t=u_i-\frac{V_p}{A_f\rho}\int_0^t\frac{1}{R_c}\frac{\mathrm{d}c_A}{\mathrm{d}t}\mathrm{d}t \tag{10}$$

where

$$\int_0^t\frac{\mathrm{d}c_A}{\mathrm{d}t}\mathrm{d}t=\frac{A}{F}(1-\mathrm{e}^{-Ft}) \tag{11}$$

The change in the mean hydraulic aperture, b, is generally different from the change in the mechanical aperture [45], since the flow domain has an intervening obstruction of relative area, R_c. Correspondingly, the change in hydraulic aperture, $\mathrm{d}b$, is related to mechanical closure, $\mathrm{d}u$, via the shortening of the asperity pedestal, as $\mathrm{d}b=(1-R_c)\mathrm{d}u$. This results in

$$b=b_i+\Delta b=b_i+\int_0^t\frac{\mathrm{d}b}{\mathrm{d}t}\mathrm{d}t=b_i-\frac{V_p}{A_f\rho}\int_0^t\left[\frac{1-R_c}{R_c}\frac{\mathrm{d}c_A}{\mathrm{d}t}-\frac{\mathrm{d}c_B}{\mathrm{d}t}\right]\mathrm{d}t \tag{12}$$

where

$$\int_0^t\frac{\mathrm{d}c_B}{\mathrm{d}t}\mathrm{d}t=-\int_0^t B(c[t]-c_{\mathrm{eq}})\,\mathrm{d}t \tag{13}$$

It is important to note that the hydraulic aperture is defined as the average over the entire area of the fracture, A_f, therefore, $V_p=A_fb$, but $\mathrm{d}u=(1/(1-R_c))\mathrm{d}b$. Finally, substituting Equation (9) into Equation (13) yields the change in aperture due to dissolution of the free face of the fracture, as

$$\int_0^t\frac{\mathrm{d}c_B}{\mathrm{d}t}\,\mathrm{d}t=B\left(c_{\mathrm{eq}}t-\frac{(B(c_0-c_{\mathrm{eq}})+Q(c_0-c_{\mathrm{in}}))}{(B+Q)^2}(1-\mathrm{e}^{-(B+Q)t})\right.$$
$$\left.-\frac{A(1-\mathrm{e}^{-Ft})}{F(B+Q-F)}+\frac{A(1-\mathrm{e}^{-(B+Q)t})}{(B+Q)(B+Q-F)}-\frac{Bc_{\mathrm{eq}}t+Qc_{\mathrm{in}}t}{B+Q}\right) \tag{14}$$

Thus, the deformation and hydraulic response of the fracture may be tracked as a consequence of both dissolution from beneath the intervening asperity anvil, and as a result of free-face dissolution or precipitation. This response may be followed for systems that are arbitrarily hydraulically open ($Q\neq0$) or closed ($Q=0$).

DOI: 10.1002/nag

2.4. Observational data

This model may be compared with behavior observed in a variety of flow-through experiments conducted on both novaculite [2, 41] and in limestone [6, 7, 46] to define the fidelity of the proposed characterization. Both the novaculite and limestone have near-zero matrix porosity, so that the full observed response is due to the fracture.

Novaculite: In this experiment, distilled water flowed through the fracture for a total of ~900 h, at relatively high flow rates ranging from 0.2 to 0.9 cc/min, and under a constant confining stress of 3.5 MPa and effective stress of ~2 MPa [2]. The system is far from equilibrium. During the experiment, the change in hydraulic aperture of the fracture is evaluated continuously from the prescribed flow rate, and measured pressure drop. The aperture drops from 12 to 3 μm with the progress of the experiment, representing a hundredfold drop in permeability, as the temperature is augmented from 20° to 80° to 120° and finally to 150°C. This behavior is shown in Figure 3 together with change in the measured efflux of Si in the first 80 h of the experiment.

Fits with these data are completed to concurrently match both the aperture change and the chemical data. These fits are shown in Figure 3 for the full experiment, and the parameters utilized for the fits are identified in Table I. The change in aperture is evaluated from Equation (12) and the corresponding change in concentration is evaluated from Equation (9). The calculated changes in aperture closely follow the observed response. Notably, the maximum closure of the fracture is well represented by the ultimate modeled closure. Where the behavior over the first 80 h is magnified, as shown in Figure 4, the match for this period, at temperatures of 20° and 80°C is quite good. Similarly, the fitting parameters of A, B and F provide consistent fits in log-linear space. Both parameters A and B remain approximately constant within the range of temperatures explored in the experiment, suggesting that the behavior of the system is consistently represented by the phenomenology of the model. The time constant for stress-driven dissolution is represented by F, and its inverse Arrhenius dependency on temperature. These dependencies are consistent with the expected dimensional response of the system.

Limestone: This flow-through experiment is similar to the prior test: total applied stress on the sample is retained constant (~3.5 MPa) as is effective stress (~2 MPa) at a fixed flow rate of 2 cc/min, but the experiment is isothermal and conducted at 20°C. The experiment was conducted in two stages: the first involving the circulation of 'groundwater' at pH ~ 8 and the second when distilled water (pH ~ 6) is then introduced. The response to this experiment has been reported elsewhere [7], and preliminary analyses completed to represent behavior [6]. Significant in the

Table I. Magnitudes of model constants for flow in Novaculite.

Temperature (°C)	A (kg m^{-3} s^{-1})	F(s^{-1})	B(s^{-1})	Q(s^{-1})*	Pore volume, V_p(m^3)†	Initial aperture, b_i(μm)	Solubility, C_{eq}(kg m^{-3})	Relative contact-area ratio, R_c (Equation (3))
20	6.0×10^{-4}	1.0×10^{-5}	1.0×10^{-5}	0.30	2.83×10^{-8}	12.0	5.43×10^{-3}	0.10
80	7.0×10^{-4}	4.0×10^{-6}	1.0×10^{-5}	0.56	2.83×10^{-8}	12.0	3.42×10^{-2}	0.10
120	6.5×10^{-4}	3.0×10^{-6}	1.0×10^{-5}	0.24	2.83×10^{-8}	12.0	8.54×10^{-2}	0.10
150	6.2×10^{-4}	2.6×10^{-6}	1.0×10^{-5}	0.14	2.83×10^{-8}	12.0	1.51×10^{-1}	0.10

*Defined as the flow rates prescribed in the experiment divided by pore volume.
†Defined as the product of initial aperture and nominal fracture area.

DOI: 10.1002/nag

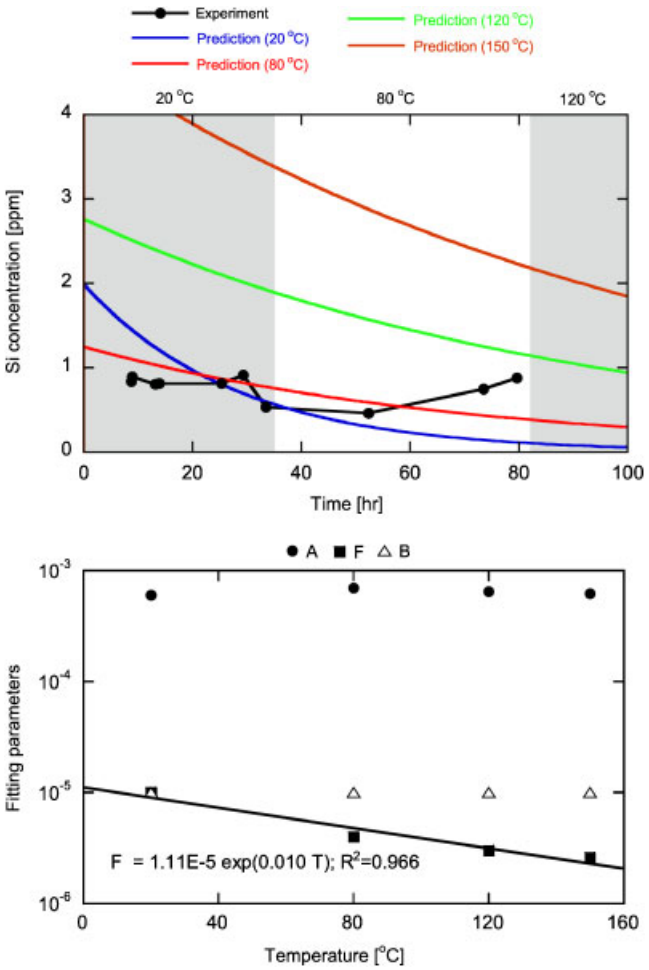

Figure 4. (Top) Change in Si concentration with time over the measured period of the experiment, shown in Figure 3. (Bottom) Change in fitting parameters A, B and F with temperature.

response is that the aperture first reduces in response to the effects of pressure solution, in response to circulation by 'groundwater'. Once the system is pushed further from the equilibrium, with the introduction of distilled water, the closure first accelerates, and then the flow impedance drops drastically as a large through-going conduit is etched through the sample [7].

The response observed in this experiment may also be matched by this model, as illustrated in Figure 5, using consistent parameters identified in Table II. The model is capable of closely replicating the aperture closure when pressure solution dominates. The matches for Ca concentrations are also adequate, but in the early period, the measurements are inadequately matched by the model [7]. Once the through-going conduit is etched (a wormhole), the simple lumped parameter model is incapable of following the response. In this instance, the implementation of such a constitutive model into a spatial model is mandatory. Only through this can the development of a strongly heterogeneous system be followed.

DOI: 10.1002/nag

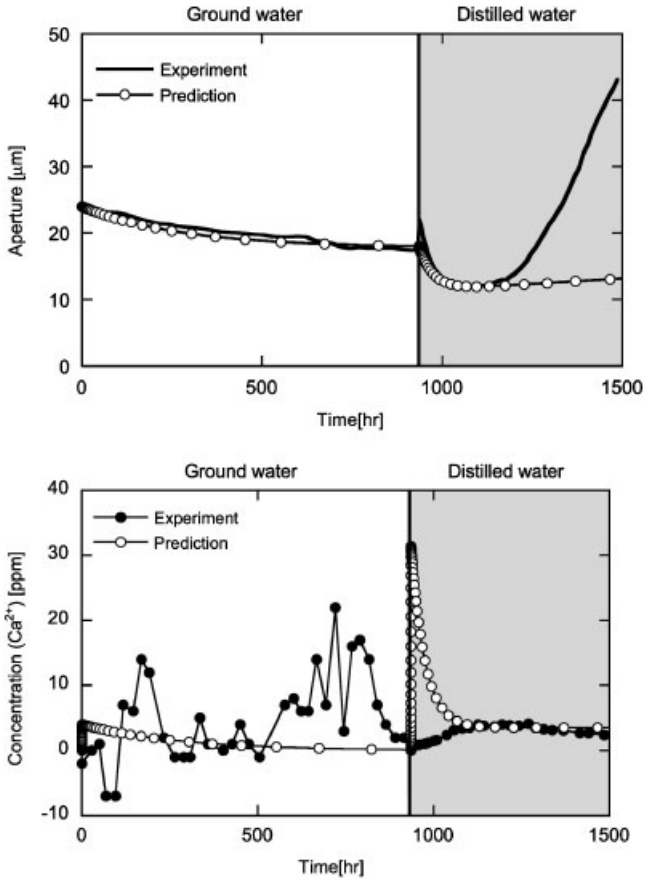

Figure 5. Comparison of experimental and model results for a 1500 h circulation test on limestone. Fitting parameters as identified in Table II. (Top) Change in aperture with time and (Bottom) change in Ca^{2+} concentration with time.

3. PARAMETRIC RESPONSE

With the capability to replicate observed responses established in the previous, anticipated features in the response to idealized hydraulically closed and open systems may be investigated. These will reveal important features in their anticipated behavior, characteristic responses and the magnitudes of various parameters which condition this response. These behaviors are examined in the following.

3.1. Closed system ($Q=0$)

Where the system is both hydraulically closed ($Q=0$), and where the dissolution at the fracture wall is discounted ($B=0$), then the equilibrium response at $t\to\infty$ may be determined from

DOI: 10.1002/nag

Table II. Magnitudes of model constants for flow in Limestone.

Permeant	A ($\mathrm{kg\,m^{-3}\,s^{-1}}$)	F ($\mathrm{s^{-1}}$)	B ($\mathrm{s^{-1}}$)	Q ($\mathrm{s^{-1}}$)*	Pore volume V_p ($\mathrm{m^3}$)†	Initial aperture, b_i (μm)	Solubility, C_{eq} ($\mathrm{kg\,m^{-3}}$)	Relative Contact-area ratio, R_c (Equation (3))
Ground water	1.2×10^{-4}	1.0×10^{-6}	1.0×10^{-3}	2.88×10^{-2}	1.30×10^{-7}	24.0	3.74×10^{-2}	0.15
Distilled water	1.2×10^{-4}	7.0×10^{-6}	4.0×10^{-4}	3.86×10^{-3}	9.72×10^{-7}	18.0	3.74×10^{-2}	0.15

*Defined as the flow rates prescribed in the experiment divided by pore volume, V_p.

†Defined as the product of initial aperture, b_i, and nominal fracture area, A_f.

Equation (9) as

$$c[\infty]\rightarrow\frac{A}{F} \tag{15}$$

For this simplest of cases, the equilibrium displacement results directly from Equation (10) as

$$u[\infty]=u_i+\Delta u=u_i-\frac{V_p}{A_f\rho}\frac{1}{R_c}\frac{A}{F} \tag{16}$$

and, again where $B=0$ only, the change in aperture is equivalent to the displacement, as implied by Equation (12) as

$$b[\infty]=b_i+\Delta b=b_i-\frac{V_p}{A_f\rho}\frac{1-R_c}{R_c}\frac{A}{F} \tag{17}$$

Where the initial equivalent hydraulic aperture (measured relative to the entire fracture area, A_f), is set to b_i, the geometry of Figure 2 defines the pore volume, V_p, as $V_p=b_iA_f$ and the displacement is given as

$$u[\infty]=u_i+\Delta u=u_i-\frac{b_i}{\rho}\frac{1}{R_c}\frac{A}{F} \tag{18}$$

or in non-dimensional form

$$u[\infty]/b_i=u_i/b_i+\Delta u/b_i=u_i/b_i-\frac{1}{\rho}\frac{1}{R_c}\frac{A}{F} \tag{19}$$

The corresponding change in aperture is

$$b[\infty]=b_i+\Delta b=b_i-\frac{b_i(1-R_c)}{\rho}\frac{1}{R_c}\frac{A}{F} \tag{20}$$

or in non-dimensional form

$$b[\infty]/b_i=b_i/b_i+\Delta b/b_i=1-\frac{(1-R_c)}{\rho}\frac{1}{R_c}\frac{A}{F} \tag{21}$$

Typical observations during experiments (see previous) are for closures to be to the order of 20% of the original aperture. Therefore, for typical contact areas of $R_c\sim\frac{1}{3}$, then $A/\rho F\sim0.1$.

DOI: 10.1002/nag

Clearly, the admissible range of non-dimensional closure is for $0<b[\infty]/b_i<1$, and for $R_c \sim \frac{1}{3}$, then this corresponds to $\frac{1}{2}>A/\rho F>0$.

Where dissolution is important, then $B \neq 0$, and although displacement will asymptote to a static magnitude of Equation (19) as $t \to \infty$, aperture will continue to change after the effects of pressure solution have been largely completed. In this instance, free-face dissolution or precipitation drives a change in aperture; the sense of this effect is controlled by the magnitude of the peak concentration (c_A) driven by pressure solution. If peak $c_A<c_{\mathrm{eq}}$ then aperture will increase with time to an equilibrium magnitude, and if $c_A>c_{\mathrm{eq}}$, then aperture will decrease. The final aperture magnitude as $t \to \infty$ is given as

$$b[\infty]=b_i+\Delta b=b_i-\frac{b_i(1-R_c)}{\rho}\left[\frac{1}{R_c}\frac{A}{F}-\frac{1}{1-R_c}\left[(c_0-c_{\mathrm{eq}})+\frac{A}{F}\right]\right] \tag{22}$$

in dimensional form, and as

$$b[\infty]/b_i=1-\frac{(1-R_c)}{\rho}\left[\frac{1}{R_c}\frac{A}{F}-\frac{1}{1-R_c}\left[(c_0-c_{\mathrm{eq}})+\frac{A}{F}\right]\right] \tag{23}$$

in non-dimensional form.

Typical behaviors for a closed system are shown in Figure 6.

3.2. *Open system* ($Q \neq 0$)

When the system is open, then $Q \neq 0$, and again the system reaches an equilibrium response in terms of a steady magnitude of the fluid concentration, $c[\infty]$. This behavior is reached, as the injection of mass controlled by pressure solution has been fully depleted, and the resulting concentration is a balance between the rate of flow and the dissolution rate from the walls, moderated by the injection and equilibrium concentrations. Thus, as $t \to \infty$, then the equilibrium effluent concentration may be determined from Equation (9) as

$$c[\infty]=\frac{Bc_{\mathrm{eq}}+Qc_{\mathrm{in}}}{(B+Q)} \tag{24}$$

where the contribution from pressure solution is absent (no A or F term) as the process has already terminated. The evolving displacement is controlled by the response to pressure solution, but once this process is complete, no further displacement will occur, unless the rock bridge is so weakened that collapse must ensue. Correspondingly, displacements are identical to those in the closed system, and are as defined by Equation (18) (originally recovered from Equation (10)), with non-dimensional displacements defined by Equation (19). However, apertures will continue to change in the presence of dissolution, and no steady state is reached, although the rate of change of aperture will approach a steady magnitude. Substituting Equation (14) into (12) yields, for the case where pressure solution effects have completed

$$b[t\to\infty]=b_i+\Delta b=b_i-\frac{V_p(1-R_c)}{A_f\rho}\left[\frac{1}{R_c}\frac{A}{F}-\frac{1}{1-R_c}\left[B\left(\frac{(B(c_0-c_{\mathrm{eq}})+Q(c_0-c_{\mathrm{in}}))}{(B+Q)^2}\right.\right.\right.$$
$$\left.\left.\left.+\frac{A}{F(B+Q-F)}-\frac{A}{(B+Q)(B+Q-F)}+\frac{Bc_{\mathrm{eq}}t+Qc_{\mathrm{in}}t}{B+Q}-c_{\mathrm{eq}}t\right)\right]\right] \tag{25}$$

DOI: 10.1002/nag

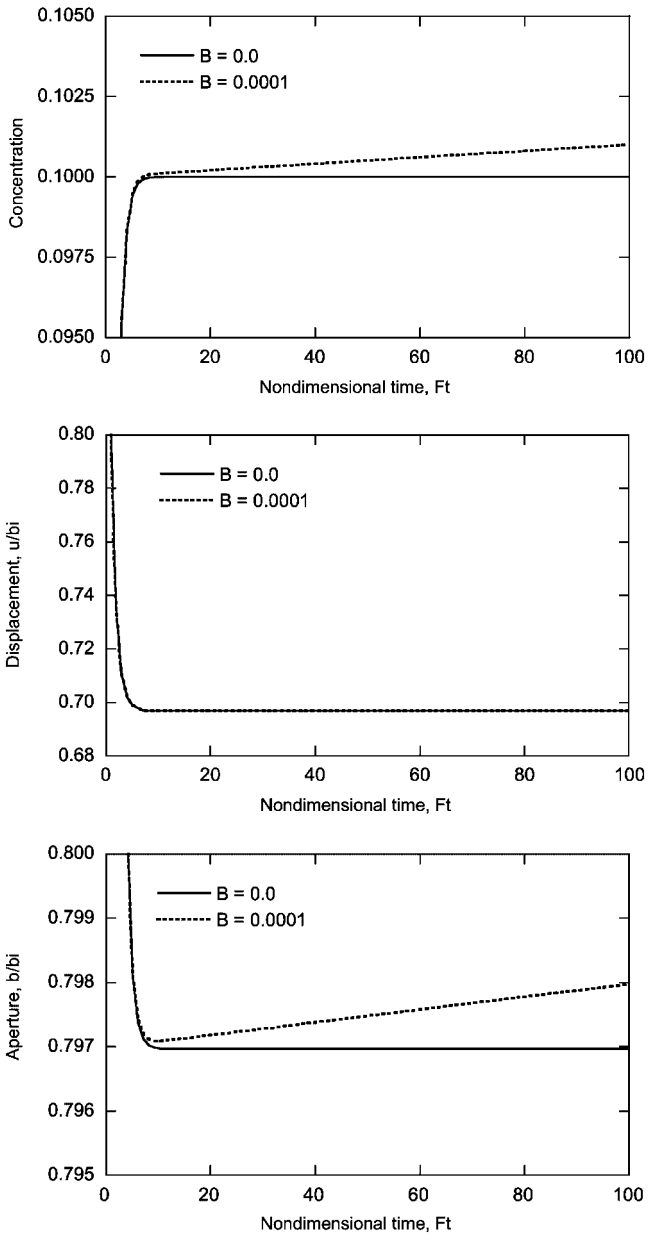

Figure 6. Response for closed system ($Q=0$) with finite dissolution. Panels show growth of concentration and evolution of displacement with time where dissolution is absent ($B=0$) and present ($B=0.0001$).

The response of an open system is shown in Figure 7. Again, the system can be followed by using the most general relationships for the evolution of concentration (Equation (9)), displacement (Equation (10)) and aperture (Equation (12)). In this, the aperture drops rapidly with the evolution of pressure dissolution, but once this process is complete, free-face dissolution overtakes this effect

DOI: 10.1002/nag

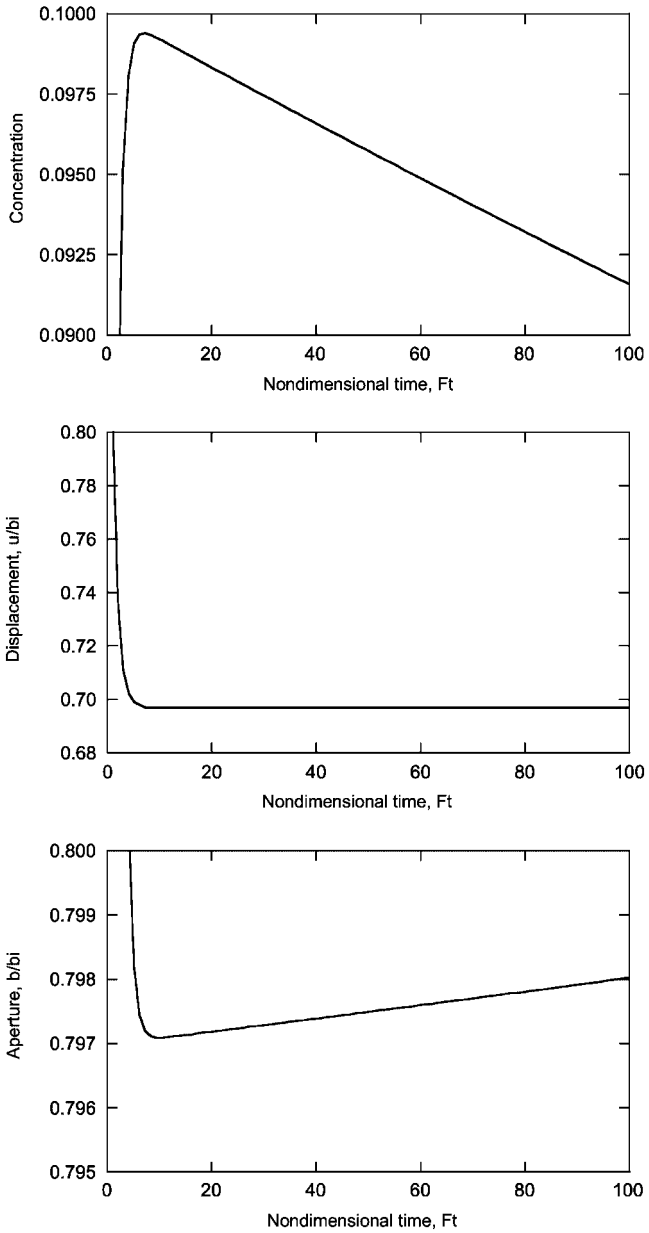

Figure 7. Response for open system ($Q = 0.0001$) with finite dissolution. Panels show growth of concentration and evolution of displacement with time.

and results in the net opening of the fracture. This gaping continues unabated, as illustrated by the straight-line portion of the response in time, although displacements will asymptote to the open system magnitudes, and concentrations will asymptote to a steady magnitude defined by Equation (24).

DOI: 10.1002/nag

4. CONCLUSIONS

A model is developed to accommodate the effects of dissolution and precipitation on the transport properties of fractures where the role of stress is appropriately accommodated. In this, changes in stresses and in temperature are able to elicit a response of preferentially mobilizing mineral mass from fracture bridges, without any supposition of the mechanism by which it may occur. It may result from the effects of increased chemical potential that results from 'pressure solution'-type effects, or it may result from the advance of sub-critical crack growth or contact undercutting or erosion at these locations. The principal requirement is that some equilibrium mineral mass is mobilized, which may then be ejected into the flow field. In this particular representation, the ejected mass is rate-controlled by dissolution, rather than thin-film diffusion, although different mechanisms can be selected which conform to this observed phenomenology.

The motivation of this analysis is to produce a continuum representation capable of capturing the essential features of the complex processes of pressure solution and dissolution/precipitation which act at the microscale. The consideration of mass continuity for the dissolved mineral mass, and the establishment for a rate law to describe precipitation or dissolution relative to the aqueous concentration of the infiltrating fluid, enables the progress of fracture sealing effects to be followed. Importantly, these considerations make feasible the response that fracture apertures may reduce, and permeabilities concomitantly fall, where mineral mass is net dissolved from the system. Alternatively, where the progress of pressure dissolution is complete, open systems circulating chemically undersaturated fluids will etch the free face and result in the gaping of fractures. These dual effects are readily accommodated in the same model. Of principal importance is the source and destination of the redistributed mineral mass within the fracture, in conditioning this response. Where prior equilibrium is disturbed by an increase in either stress or temperature, mineral mass is injected into the aqueous system, and correspondingly reduces the aperture. This reduction in aperture is time dependent, with a characteristic time controlled by the destruction of the fracture bridge. Overprinted on this response is the influence of the mass ejected from the fracture bridge. In a closed system, originally at aqueous equilibrium, this mineral mass is trapped within the REV of the fracture and will precipitate on the fracture walls, additively reducing the aperture. In an open system, this mass will be added to the interstitial fluid, and depending on the influent chemistry, will affect the response of the system in a variety of ways—apertures must initially drop, but will subsequently either build or continue to drop, depending on the specifics of the flow system. Thus, the full variety of complex behaviors observed in such systems pushed far-from-equilibrium may be followed, depending on the initial and boundary conditions applied to the system. These models are applied to observational data for open systems, far-from-equilibrium, where both closure and gaping of the fractures are observed, and satisfactory agreement obtained. The models are an essential step in representing the observed macroscopic response at the microscale at the continuum macroscopic scale.

ACKNOWLEDGEMENTS

This work is as a result of partial support from the US Department of Energy under grant DE-AC02-05CH11231 and the National Science Foundation under grant EAR-0510182. This support is gratefully acknowledged. The conclusions reported here are those of the authors.

DOI: 10.1002/nag

REFERENCES

1. Daily W, Lin W, Buscheck T. Hydrological properties of topopah spring tuff—laboratory measurements. *Journal of Geophysical Research—Solid Earth and Planets* 1987; **92**(B8):7854–7864.
2. Polak A *et al.* Permeability reduction of a natural fracture under net dissolution by hydrothermal fluids. *Geophysical Research Letters* 2003; **30**(20):2020. DOI: 10.1029/2003GL017575.
3. Lin WN, Daily W. Hydrological properties of topopah spring tuff under a thermal-gradient—laboratory results. *International Journal of Rock Mechanics and Mining Sciences and Geomechanics Abstracts* 1990; **27**(5):373.
4. Moore DE, Lockner DA, Byerlee JD. Reduction of permeability in granite at elevated-temperatures. *Science* 1994; **265**(5178):1558–1561.
5. Sevougian SD, Schechter RS, Lake LW. Effect of partial local equilibrium on the propagation of precipitation dissolution waves. *Industrial and Engineering Chemistry Research* 1993; **32**(10):2281–2304.
6. Liu JS *et al.* Dissolution-induced preferential flow in a limestone fracture. *Journal of Contaminant Hydrology* 2005; **78**(1–2):53–70.
7. Polak A *et al.* Spontaneous switching of permeability changes in a limestone fracture with net dissolution. *Water Resources Research* 2004; **40**(3):1016.
8. Groves CG, Howard AD. Minimum hydrochemical conditions allowing limestone cave development. *Water Resources Research* 1994; **30**(3):607–615.
9. Karcz Z, Scholz CH. The fractal geometry of some stylolites from the Calcare Massiccio formation, Italy. *Journal of Structural Geology* 2003; **25**(8):1301–1316.
10. Singurindy O, Berkowitz B. Evolution of hydraulic conductivity by precipitation and dissolution in carbonate rock. *Water Resources Research* 2003; **39**(1):1016. DOI: 10.1029/2001WR001055.
11. Singurindy O, Berkowitz B. The role of fractures on coupled dissolution and precipitation patterns in carbonate rocks. *Advances in Water Resources* 2005; **28**(5):507–521.
12. Aharonov E, Tenthorey E, Scholz CH. Precipitation sealing and diagenesis—2. Theoretical analysis. *Journal of Geophysical Research—Solid Earth* 1998; **103**(B10):23969–23981.
13. Chester JS *et al.* Mechanisms of compaction of quartz sand at diagenetic conditions. *Earth and Planetary Science Letters* 2004; **220**(3–4):435–451.
14. de Meer S, Spiers CJ, Nakashima S. Structure and diffusive properties of fluid-filled grain boundaries: an in-situ study using infrared (micro) spectroscopy. *Earth and Planetary Science Letters* 2005; **232**(3–4):403–414.
15. Groshong RH. Low-temperature deformation mechanisms and their interpretation. *Geological Society of America Bulletin* 1988; **100**(9):1329–1360.
16. Elias BP, Hajash A. Changes in quartz solubility and porosity due to effective stress—an experimental investigation of pressure solution. *Geology* 1992; **20**(5):451–454.
17. Hickman SH, Evans B. Kinetics of pressure solution at halite–silica interfaces and intergranular clay films. *Journal of Geophysical Research—Solid Earth* 1995; **100**(B7):13113–13132.
18. Niemeijer A, Spiers CJ, Bos B. Compaction creep of quartz sand at 400–600 degrees C: experimental evidence for dissolution-controlled pressure solution. *Earth and Planetary Science Letters* 2002; **195**(3–4):261–275.
19. Gratier JP. Experimental pressure solution of halite by an indenter technique. *Geophysical Research Letters* 1993; **20**(15):1647–1650.
20. Hajash A, Carpenter TD, Dewers TA. Dissolution and time-dependent compaction of albite sand: experiments at 100 degrees C and 160 degrees C in pH-buffered organic acids and distilled water. *Tectonophysics* 1998; **295**(1–2):93–115.
21. Renard F *et al.* Three-dimensional roughness of stylolites in limestones. *Journal of Geophysical Research—Solid Earth* 2004; **109**(B3):B3209.
22. Renard F *et al.* Enhanced pressure solution creep rates induced by clay particles: experimental evidence in salt aggregates. *Geophysical Research Letters* 2001; **28**(7):1295–1298.
23. Renard F, Ortoleva P, Gratier JP. Pressure solution in sandstones: influence of clays and dependence on temperature and stress. *Tectonophysics* 1997; **280**(3–4):257–266.
24. Cox SF, Paterson MS. Experimental dissolution–precipitation creep in quartz aggregates at high-temperatures. *Geophysical Research Letters* 1991; **18**(8):1401–1404.
25. Renard F, Gratier JP, Jamtveit B. Kinetics of crack-sealing, intergranular pressure solution, and compaction around active faults. *Journal of Structural Geology* 2000; **22**(10):1395–1407.
26. Tenthorey E *et al.* Precipitation sealing and diagenesis—1. Experimental results. *Journal of Geophysical Research—Solid Earth* 1998; **103**(B10):23951–23967.

27. Zhang SQ, Paterson MS, Cox SF. Microcrack growth and healing in deformed calcite aggregates. *Tectonophysics* 2001; **335**(1–2):17–36.
28. Bos B, Peach CJ, Spiers CJ. Slip behavior of simulated gouge-bearing faults under conditions favoring pressure solution. *Journal of Geophysical Research—Solid Earth* 2000; **105**(B7):16699–16717.
29. Bos B, Spiers CJ. Frictional-viscous flow of phyllosilicate-bearing fault rock: microphysical model and implications for crustal strength profiles. *Journal of Geophysical Research—Solid Earth* 2002; **107**(B2):2028. DOI: 10.1029/2001/JB000301.
30. Claesson L *et al.* Hydrogeochemical changes before and after a major earthquake. *Geology* 2004; **32**(8):641–644.
31. Gratier JP, Favreau P, Renard F. Modeling fluid transfer along California faults when integrating pressure solution crack sealing and compaction processes. *Journal of Geophysical Research—Solid Earth* 2003; **108**(B2):2104. DOI: 10.1029/2001JB000380.
32. Gratier JP *et al.* Fluid pressure evolution during the earthquake cycle controlled by fluid flow and pressure solution crack sealing. *Earth Planets and Space* 2002; **54**(11):1139–1146.
33. Kanagawa K, Cox SF, Zhang SQ. Effects of dissolution–precipitation processes on the strength and mechanical behavior of quartz gouge at high-temperature hydrothermal conditions. *Journal of Geophysical Research—Solid Earth* 2000; **105**(B5):11115–11126.
34. Kay MA *et al.* Fault gouge diagenesis at shallow burial depth: solution-precipitation reactions in well-sorted and poorly sorted powders of crushed sandstone. *Earth and Planetary Science Letters* 2006; **243**(3–4):607–614.
35. Nakatani M, Scholz CH. Frictional healing of quartz gouge under hydrothermal conditions: 1. Experimental evidence for solution transfer healing mechanism. *Journal of Geophysical Research—Solid Earth* 2004; **109**(B7):B07201. DOI: 10.1029/2001JB001522.
36. Tenthorey E, Cox SF, Todd HF. Evolution of strength recovery and permeability during fluid–rock reaction in experimental fault zones. *Earth and Planetary Science Letters* 2003; **206**(1–2):161–172.
37. Ojala IO, Ngwenya BT, Main IG. Loading rate dependence of permeability evolution in porous aeolian sandstones. *Journal of Geophysical Research—Solid Earth* 2004; **109**(B1):B01204. DOI: 10.1029/2002JB002347.
38. Zhang SQ, Cox SF, Paterson MS. The influence of room-temperature deformation on porosity and permeability in calcite aggregates. *Journal of Geophysical Research—Solid Earth* 1994; **99**(B8):15761–15775.
39. Yasuhara H, Elsworth D, Polak A. A mechanistic model for compaction of granular aggregates moderated by pressure solution. *Journal of Geophysical Research—Solid Earth* 2003; **108**(B11):2530. DOI: 10.1029/2003JB002536.
40. Durham WB, Bourcier WL, Burton EA. Direct observation of reactive flow in a single fracture. *Water Resources Research* 2001; **37**(1):1–12.
41. Yasuhara H, Elsworth D, Polak A. Evolution of permeability in a natural fracture: significant role of pressure solution. *Journal of Geophysical Research—Solid Earth* 2004; **109**(B3):B03204. DOI: 10.1029/2003JB002663.
42. Yasuhara H *et al.* Evolution of fracture permeability through fluid–rock reaction under hydrothermal conditions. *Earth and Planetary Science Letters* 2006; **244**(1–2):186–200.
43. Tada R, Siever R. Pressure solution during diagenesis. *Annual Review of Earth and Planetary Sciences* 1989; **17**:89–118.
44. Siddiqi G *et al.* Effect of semibrittle deformation on transport properties of calcite rocks. *Journal of Geophysical Research—Solid Earth* 1997; **102**(B7):14765–14778.
45. Piggott AR, Elsworth D. Laboratory assessment of the equivalent apertures of a rock fracture. *Geophysical Research Letters* 1993; **20**(13):1387–1390.
46. Liu JS *et al.* A fully coupled hydrological–mechanical–chemical model for fracture sealing and preferential opening. *International Journal of Rock Mechanics and Mining Sciences* 2006; **43**(1):23–36.